Laser melt injection in aluminum alloys: On the role of the oxide skin

Vreeling, Jan; Ocelik, V.; Pei, Y.T.; van Agterveld, Dimitri; de Hosson, J.T.M.

Published in:
Acta Materialia

DOI:
10.1016/S1359-6454(00)00278-0

Publication date:
2000

Pergamon

Acta mater. 48 (2000) 4225–4233

Acta MATERIALIA

www.elsevier.com/locate/actamat

LASER MELT INJECTION IN ALUMINUM ALLOYS: ON THE ROLE OF THE OXIDE SKIN

J. A. VREELING, V. OCELíK, Y. T. PEI, D. T. L. VAN AGTERVELD and J. Th. M. DE HOSSON*

Department of Applied Physics, Materials Science Center and Netherlands Institute for Metals Research, University of Groningen, Nijenborgh 4, 9747 AG Groningen, The Netherlands

(Received 17 April 2000; received in revised form 11 July 2000; accepted 3 August 2000)

Abstract—In this paper the method of laser melt injection of SiC particles into an aluminum substrate is investigated both experimentally and theoretically. An extremely small operational parameter window was found for successful injection processing. It is shown that the final injection depth of the particles is controlled mainly by the temperature of the melt pool rather than by the particle velocity. A theoretical model that takes into account the wetting behavior and the particle penetration processes is developed on the basis of the observed particle velocity, thickness and area fraction of oxide skin that partially covers the surface of the heated aluminum melt pool. The model reveals the role of the oxide skin: it is relatively strong at low temperature and acts as a severe barrier for the injection process. It was found that preheating the aluminum substrate results in a higher temperature of the melt pool and partial dissolution of the oxide skin, through which the injected particles are able to penetrate.

Keywords: Powder processing; Scanning electron microscopy (SEM); Auger electron microscopy; Aluminum alloys; Oxidation

1. INTRODUCTION

Treatments of metal surfaces with high-power lasers are appropriate for improving the mechanical, tribological and chemical properties of metallic surfaces [1]. The laser melt injection (LMI) method [2–6] is aimed at producing a metal-matrix composite (MMC) layer on top of a substrate. The laser beam melts the substrate locally while simultaneously injecting particles of additional material (usually ceramics). These particles are trapped when the melt pool rapidly resolidifies after the laser beam has passed. In the commonly applied laser cladding process a coating is created by fully melting the additional powder material and forming a new alloyed layer after mixture with the substrate material. Unlike laser cladding [7], the contact between laser beam and added material in LMI is limited to the level that is just necessary to form strong bonding interface between the ceramic particles and the metallic matrix in the final MMC layer.

During laser treatments of aluminum alloys one has to face certain problems [8]. For the wavelength of radiation produced by an Nd:YAG laser (λ = 1.06 μm), as used in this work, the reflectivity of solid Al is about 90% [9]. Therefore a high energy density of the laser beam is needed to create a melt pool in Al. Another problem is the oxide skin that is naturally formed on an Al melt. This oxide layer on molten Al has a substantial influence on the wetting behavior of ceramic particles with liquid Al [10]. Usually, the oxide skin forms an energy barrier for the particles to penetrate. However, the strength of this barrier depends on the temperature of the melt pool. For instance, at lower temperatures (640–850°C), the contact angle between an SiC particle and the Al melt is about 130°, while at higher temperatures (>1100°C) the contact angle is decreased to about 50° [10].

In this work the LMI method was scrutinized for the SiC_p/Al system. Experimentally observed phenomena are discussed within the framework of the laser process, and the microstructural features are supported by a theoretical analysis.

* To whom all correspondence should be addressed. Tel.: +31 50 363 4898; fax: +31 50 363 4881.

E-mail address: hossonj@phys.rug.nl (J.T.M. De Hosson)

1359-6454/00/$20.00
PII: S1359-6454(00)00278-0

2. EXPERIMENTAL PROCEDURES

The laser experiments were carried out with a continuous wave, 2 kW Rofin Sinar Nd:YAG laser. The laser beam is positioned at an angle of 11° with respect to the substrate surface normal to avoid harmful reflections from the specimen back into the optical fiber. Ar was used as a shielding gas to protect the lens as well as to reduce oxidation of the specimen. The spot size of the laser beam on the workpiece was 2.4 mm. A computer numerically controlled *X–Y* table was employed for specimen movement.

Aluminum plates with 99.6 wt% purity and dimensions of 100 mm×40 mm×10 mm were used as substrate material. Before laser treatment the surface was sand-blasted to promote absorption of the laser light [9]. A Metco 9MP powder feeding system supplied the 6H-SiC particles with mean size of about 80 μm, using Ar as a carrier gas with flow rates in the interval of 25–67 ml/s. The particles were injected into the melt pool at an angle of 35° with respect to the surface normal. The injection velocity of the SiC particles was measured by recording their flight out of the powder nozzle with a Kodak 4540 Ektapro High Speed Camera.

The temperature of the substrate, just before and during the laser processing, was acquired by a Sensys monochromatic optical pyrometer. The optical sensor was focused on the center of the border of the substrate block.

The coatings were observed with standard optical microscopy (Olympus Vanox-AHTM microscope) and scanning electron microscopy [SEM; Philips XL-30 field-emission gun (FEG) scanning electron microscope]. The oxidation layer was analyzed by a special, small-spot, ultrahigh vacuum (UHV) scanning electron/scanning Auger microscope (SEM–SAM) based on a JEOL JAMP 7800F, in which depth profiling was performed *in situ* by 1 keV Ar^+-ion bombardment.

3. RESULTS

3.1. The laser melt injection process

The experimental set-up of the laser melt injection process is displayed in Fig. 1. A powder feed apparatus connected to a cyclone makes a constant particle flow. Important is the direction of the particle flow with respect to the moving direction of the substrate. In this case the so-called "over-hill" direction is used, where the particles are traveling over the coating towards the center of the melt pool. To achieve injection conditions for SiC particles into an Al melt, the upper carrier gas outlet of the cyclone is partially or fully closed with the aim of increasing the speed of SiC particles. This also helps to reduce the interaction time between the laser beam and SiC_p, which is important because SiC has a high absorption of the laser radiation [11, 12]. For the same reason the focal point of the laser beam lies 6 mm below the substrate surface, which results in lower beam energy densities just above the surface where injected particles come into contact with the laser beam.

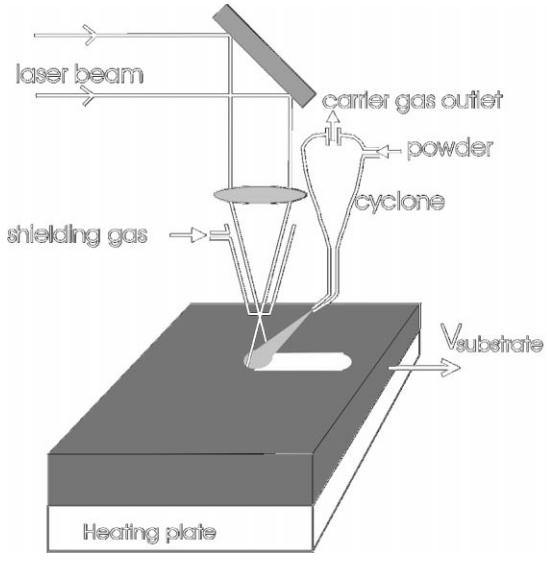

Fig. 1. Schematic picture of the laser melt injection process. The particles are injected in the so-called "over-hill" direction.

An appropriate combination of process parameters for the production of a single laser track (see Fig. 2), was found: laser beam power density of 310 MW/m^2, scanning speed 8.3 mm/s, powder feed rate 8.3 mg/s, glass nozzle diameter 1.7 mm and 60 ml/s carrier gas flow. Before the LMI process, the substrate is preheated to 300°C by a plate heater with a constant temperature and it is kept on the heater during injection. The temperature of the Al substrate increases to about 30°C after one track due to the absorbed beam energy, which provides the possibility of setting different preheating temperatures. The injection process is sensitive to small changes in power density, preheating temperature, powder flow and particle velocity, which results in an extremely small operational window of laser and powder flow parameters.

As Fig. 2 demonstrates, the SiC volume fraction in the MMC track is about 35%, and the width of the

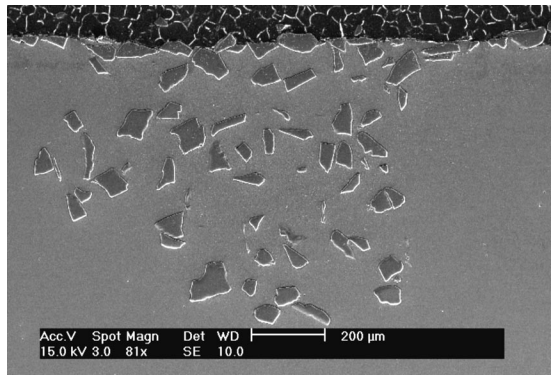

Fig. 2. SEM micrograph of the cross-section of a laser track with injected SiC particles.

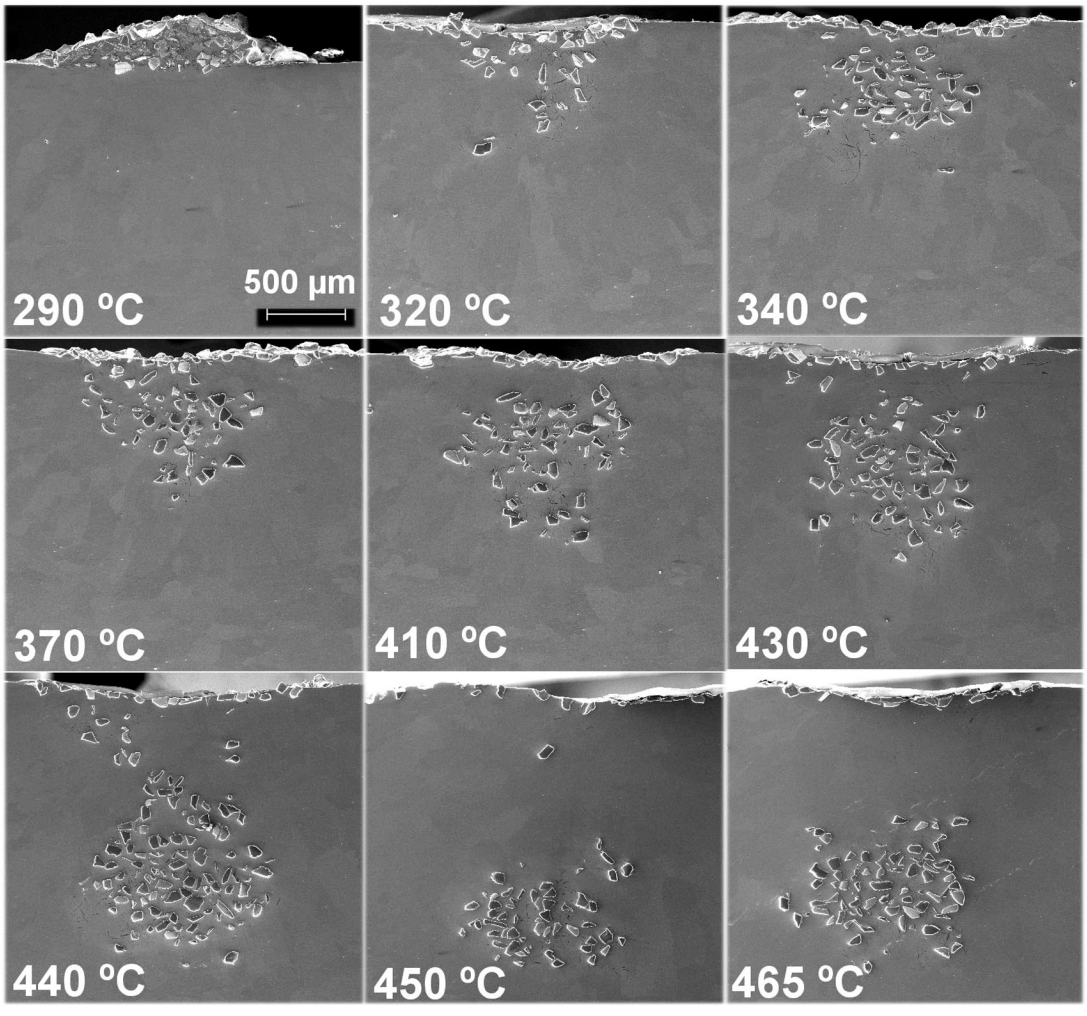

Fig. 3. Cross-sections of single laser tracks that were produced at different preheating temperatures. The SiC particles are injected above 300°C, and the higher the preheating temperature, the deeper the particles are injected. The particles are not injected across the melt pool; at the edges no particles are injected.

track is about 1 mm. The penetration depth of the injected particles depends strongly on the temperature of the melt pool, as shown in Fig. 3. When the preheating temperature is lower than 300°C the particles are not able to penetrate in the melt pool, whereas at higher temperatures the particles are successfully injected. Increasing the preheating temperature results in more, and also much deeper, injected particles. In all experiments, the melt pool was wider than the area where particles were injected.

The effect of the melt pool temperature on the injection depth is also shown in a longitudinal cross-section (Fig. 4). During the production of a laser track with a length of about 30 mm, the substrate temperature is gradually increasing and therefore the particles are injected deeper near the end of the laser track. The increase in temperature during a single laser track depends on the length of the track and the size of the substrate, which acts as a heat sink. In the case of Fig. 4 the substrate temperature increase is about 30°C, measured on the side rim of the substrate block. Besides an increase to a maximum injected depth near the end of the track, also local oscillations in the depth of injected particles are observed.

3.2. Calculation of particle penetration

A simple model is constructed for a better understanding of the particle penetration process. The prob-

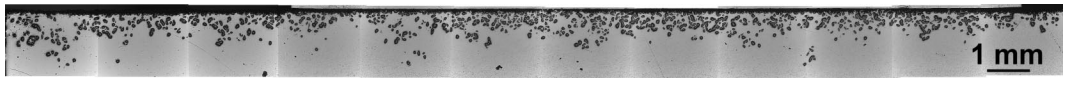

Fig. 4. Longitudinal cross-section of a laser track. The laser beam proceeded from right to left. The tendency to increase the injection depth as well as the local oscillations in the maximal injection depths is demonstrated.

lem can be divided in two parts: penetration through the melt surface and movement of the particles in a liquid. To simplify the problem the particle is assumed to be of spherical shape, having radius R and vertical component of velocity v_0. The energy the particle uses in order to overcome the molten surface barrier and to propagate further into the melt is its kinetic energy:

$$E_{\text{kin}} = \frac{2}{3}\pi R^3 \rho_{\text{SiC}} v_0^2, \tag{1}$$

where ρ_{SiC} is the density of SiC (3217 kg/m^3).

The total interface energy for a particle partially immersed in a melt at depth x, $0 \le x \le 2R$ (see Fig. 5), is given by [13]:

$$G_{\text{interface}} = (R-x)^2\pi\sigma_{\text{lv}} + 2R\pi x\sigma_{\text{lp}} + 2R\pi(2R-x)\sigma_{\text{pv}}, \tag{2}$$

where σ is the interface energy (tension) between the phases indicated by the indices l = liquid Al, p = solid SiC particle and v = vapor. The equilibrium depth x_{eq} and contact angle Θ can be calculated from equation (2) by minimizing the interface energy:

$$x_{\text{eq}} = R\frac{(\sigma_{\text{lv}} + \sigma_{\text{pv}} - \sigma_{\text{lp}})}{\sigma_{\text{lv}}} \quad \text{and} \tag{3}$$

$$\Theta = 90^\circ + \arcsin\left(\frac{R-x_{\text{eq}}}{R}\right).$$

This is basically the same as Young's equation for the equilibrium contact angle. The strength of the surface barrier can be estimated by the amount of change in interface energy when a single particle is moved from the depth where the interface energy of the system is minimal, i.e., the wetting angle, to the depth where the particle is entirely inside the melt:

$$\Delta G_{\text{barrier}} = G_{(x = x_{\text{eq}})} - G_{(x = 2R)} = \frac{(\sigma_{\text{lv}} + \sigma_{\text{lp}} - \sigma_{\text{pv}})^2}{\sigma_{\text{lv}}}\pi R^2. \tag{4}$$

Combining equations (1) and (4), the minimal vertical velocity of the particle v_{min} needed to overcome the melt surface barrier can be obtained:

$$v_{\text{min}} = \sqrt{\frac{3}{2\sigma_{\text{lv}} R\rho_{\text{SiC}}}}(\sigma_{\text{lv}} + \sigma_{\text{lp}} - \sigma_{\text{pv}}). \tag{5}$$

If the initial particle velocity is higher than v_{min}, the particle overcomes the surface barrier and may propagate further into the melt with the reduced velocity v

$$v = \sqrt{v_0^2 - v_{\text{min}}^2}, \tag{6}$$

Stoke's force

$$F = 6\pi\eta R v \tag{7}$$

and gravity corrected by Archimedes' principle, which work against each other, driving the particle penetration further. The quantity η in equation (7) denotes the viscosity of the Al melt. The values of the interface energies for both oxidized and unoxidized surfaces of liquid Al are given in Table 1 [14]. All of this indicates that the velocity of the particles and the particular state of the melt pool surface play important roles in the actual laser melt injection process.

3.3. Velocity of injected particles

A high-speed camera was used to monitor the flight of the particles after they left the nozzle, to enable their velocity to be measured and hence their kinetic energy to be calculated. Experiments with different glass nozzle diameters (ϕ = 1.7 and 2.3 mm) and different carrier gas flows (25–70 ml/s) were recorded with a camera speed of 27×10^3 frames/s. Afterwards, the particle velocity was measured on the video screen with the standard frame speed of 25 frames/s by counting the number of frames that a particle needed to travel between two markers at constant distance. The velocities of more than 50 particles were traced in each experiment.

The results of the high-speed camera observations

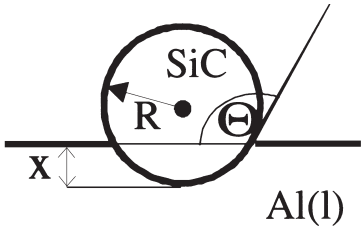

Fig. 5. A spherical SiC particle immersed in an Al melt at depth x corresponding with a contact angle Θ.

Table 1. Interface energies of oxidized and unoxidized Al in the Al(l)/SiC$_p$ system [14]

Physical quantity	Interface energy at 900 K (mJ/m^2)	
	Al oxidized	Al unoxidized
σ(SiC, solid–vapor)	1920	1920
σ(Al, liquid–vapor)	870	1100
σ(liquid Al–solid SiC)	2480	1210

are summarized in Fig. 6. The mean velocity of the particles shows a linear increase with carrier gas flow rate. A nozzle diameter of 1.7 mm increases the velocity by a factor of about 1.5, with respect to a nozzle diameter of 2.3 mm. The variation in particle speed is about 15–20%. Distinction is made between particles traveling in the upper, central and lower part of the powder stream. The particles have the highest velocity in the center of the stream; at the higher and lower parts of the stream, the velocity is about 90% of the velocity in the center. In our LMI experiments the particle velocities vary in the range of 2.5–5 m/s.

3.4. Oxide layer on aluminum

To get an idea of the behavior of the oxide layer during the laser process, single laser tracks were produced with the same laser parameters as in the injection experiments but without particle flow. The surface of a track displayed two different appearances. In the center there is a shiny strip with width of about 1.1 mm, while at both sides rather dull strips are present with an approximate width of 0.2 mm. The borders between these areas are quite sharp. FEG SEM micrographs taken on both the center and the side areas are shown in Fig. 7. In the central area of the laser track about 45–50% of the surface is not covered by a thick oxide layer. On the other hand, only 20% of the surface is not covered at the edge of the melt pool.

The thickness of the oxide layers in different areas was analyzed by depth profiling in the UHV SEM–SAM. Ar^+-ion bombardment removed the surface layer, while after each etching step the intensities of Al, O and C element peaks in Auger electron spectra were analyzed. In this way the thickness of the oxide layer can be estimated by recording the etching time that is needed to remove the oxygen from the spectra.

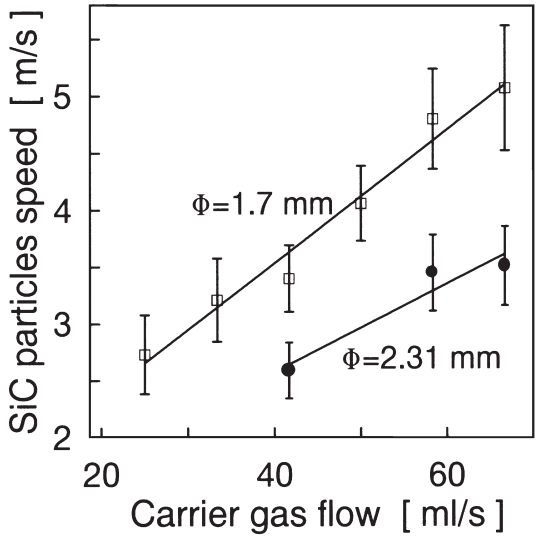

Fig. 6. Particle velocity as a function of carrier gas flow for two diameters of glass nozzle, obtained by high-speed camera observations.

The results are depicted in Fig. 8(a), (b) and (c), which presents the depth profiles measured at the locations defined in Fig. 7. It is clear that the oxide layer from the uncovered area at the center of the laser track is removed after 100–150 s of Ar^+-ion bombardment, as shown in Fig. 8(a). To remove the oxide layer from the uncovered edge region an etching time of about 800 s is necessary [Fig. 8(b)] and removal of the oxide layer from the covered edge region needs more than 5000 s [Fig. 8(c)]. From these etching times an estimate of the thickness of oxide layer can be made [15] if one knows the principal etching parameters and the so-called sputtering yield [16]. Such estimates for all three characteristic locations are marked in Fig. 8 by dashed lines.

4. DISCUSSION

The first point of discussion concerns the laser melt injection process itself. The powder stream is suitable to produce tracks of laser melt particles and the particle velocity in the powder stream is quite constant, which can be adjusted by the nozzle diameter and carrier gas flow. The extremely small operational window of laser and powder flow parameters can be explained by the substantial difference between the absorptivity of laser radiation of Al and SiC on one hand and the oxide skin of Al on the other. A high laser energy input is needed to create a melt pool in Al while the same energy input will heat up the particles enormously, when they travel through the laser beam, due to their high absorptivity for laser radiation [11, 12]. This will damage the particles and lead to undesired Al_4C_3 formation [6, 17, 18] which may have a negative effect on the mechanical properties of the coating [19]. Another effect of the high absorptivity is that the powder flow shields the surface. Therefore the feed rate should be low in comparison to the standard cladding parameters [20].

Preheating the substrate makes the laser process much more efficient because the coupling between the laser light and the substrate increases with increasing temperature. Furthermore, when the substrate is preheated to 300°C, the heating up to the melting temperature (660°C), where most of the laser light is reflected, is about halved. Although all of this explains why, by using the same laser energy, the melt pool temperature is higher when the substrate is preheated, it is hard to believe that this is the reason why preheating is essential for an appropriate particle injection process. For example, the particles are injected to a depth of 500 μm in the case of preheating to 340°C whereas they are hardly injected at a preheating temperature of 300°C. In order to understand this we shall focus on the role of the oxide skin.

It is necessary to emphasize that the measured fractions and thicknesses of the oxide surfaces *after* the laser process are probably not the same as they were *during* the laser process on the Al melt. To a first approximation it is reasonable to assume that the

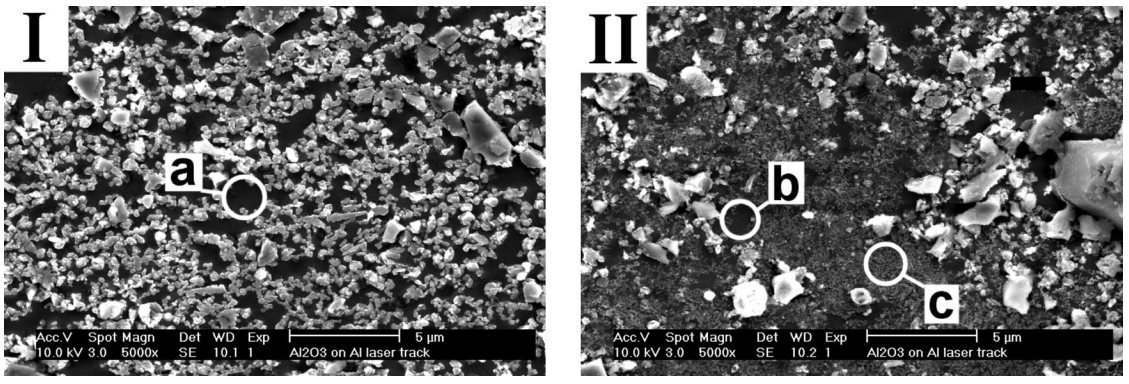

Fig. 7. SEM micrographs of two different areas on the aluminium surface after laser processing: (I) in the center of the laser track where the open areas (a) represent approximately 50% of the whole surface; (II) at the edge of the melt pool where the open parts of the surface are covered with a "spongy"-looking phase (c). Open areas (b) represent approximately 20% of the whole surface.

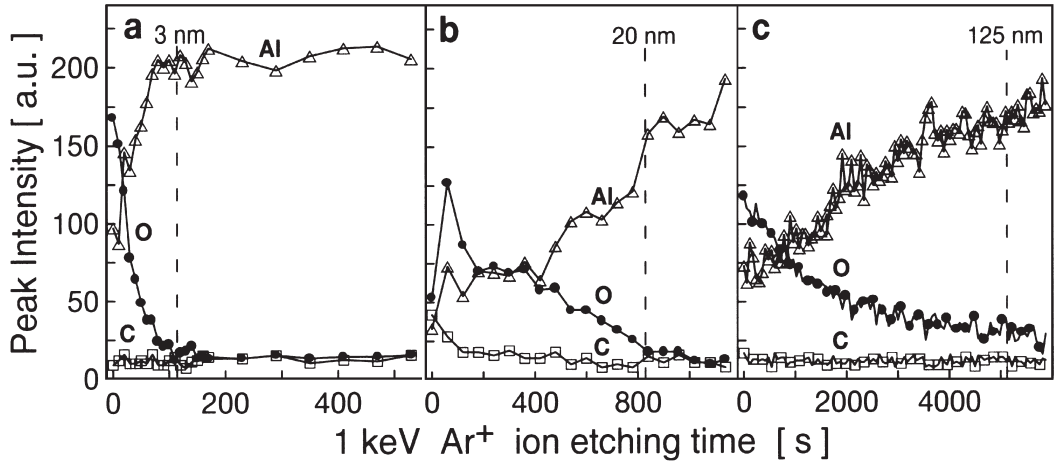

Fig. 8. Aluminium, oxygen and carbon element peak intensities in AES spectra as a function of Ar^+-ion bombardment time, giving an element depth profile. (a), (b) and (c) show the depth profiles measured at the corresponding marked areas on Fig. 7.

areas where an oxide layer of 3 nm is detected by UHV SEM–SAM did not possess any oxide layer during the laser experiments. This is because a 3 nm thick oxide layer is typical for an amorphous oxide skin reported as a layer grown on a solid Al surface [21]. In addition, the fraction of "open" areas may be higher during the laser treatments. Nevertheless, the *ex situ* experiments underline the behavior of this oxide skin as a function of temperature [10]. Actually the oxide skin, present on the melt until 850°C, prevents a direct contact between the particles and Al liquid and leads to non-wetting behavior. Above this temperature chemical interactions between Al and its oxide at the interface may occur, leading to the formation of gaseous sub-oxides. Consequently the Al surface takes over at temperatures above 850°C, allowing the particles to have direct contact with the Al liquid. This results in chemical interactions between the particle and the Al melt. These interactions lower the energy of the particle/Al interface and result in an improved wetting behavior. At about 1100°C the oxide is completely removed and consequently a transition from non-wetting to wetting behavior takes place in a small temperature interval between 850°C and 1100°C. In this interval the surface is partially covered with oxide.

The energy barrier of partially covered surfaces can be obtained, realizing that the particle size ($R =$ 40 µm) is much larger than the oxide-free parts ($<$ 5 µm in Fig. 7), by adjusting equation (4):

$$\Delta G_{\text{barrier}} = \frac{[a\sigma_{\text{lv,ox}} + a\sigma_{\text{lp,ox}} + (1-a)\sigma_{\text{lv,al}} + (1-a)\sigma_{\text{lp,al}} - \sigma_{\text{pv}}]^2}{a\sigma_{\text{lv,ox}} + (1-a)\sigma_{\text{lv,al}}} \pi R^2, \tag{8}$$

where a is the area fraction of the surface that is covered with an oxide skin, and indices ox and al indicate the interface energies of the oxidized and unoxidized case, respectively. Equation (5) can be

modified in the same way to calculate the minimum velocity to overcome the surface energy barrier; i.e., not only in the case of clean and fully covered surfaces, but also in the case of a partially covered surface. Figure 9 displays the dependence of the minimum velocity required to overcome the barrier as a function of particle size for different percentages of oxide coverage. Here, curves are depicted which characterize a surface that is fully covered, together with two experimentally observed partially covered surfaces and a surface that is free of an oxide skin. Also, the area corresponding to the particle velocities and sizes used in the injection experiments is marked in Fig. 9.

One may conclude that for 50% coverage, which is characteristic for near the center of the laser track, a velocity of about 4 m/s is sufficient to penetrate the surface layer. On the other hand, if 80% or more of the surface is covered with an oxide layer, the particles cannot be injected with the present experimental arrangements. This kind of behavior was observed in our experiments, where particles were injected only in the central part of the laser track and not near the sides. The distribution of the injected depth observed in the cross-sections of the laser track (Fig. 2) is not controlled by the distribution of the particle speed across the particle stream, but is determined by the increase of coverage with oxide from the center of the laser track to its sides.

Figure 9 also clearly indicates that laser injection is not a suitable technique for the preparation of SiC/Al MMCs with particles smaller than $R = 20$ μm. A preplacement technique is reported to be successful for particles with a size smaller than 45 μm [22, 23].

The effects of the oxide skin on the laser melt injection process will be discussed in more depth in the following. Included in the second part of the injection problem, i.e., a particle moving in a liquid, we have calculated the injection depth as a function of time. The result of such a calculation is displayed in Fig. 10 for a particle with a radius of 40 μm, an initial velocity of 4 m/s and with 50% of the surface covered by an oxide skin. The particle reaches its equilibrium velocity within 0.01 s. This velocity is very small and therefore we may assume that the particle already gains its final depth in this short time interval. The viscosity is taken to be constant in the calculations, that for Al liquid at 927°C: 0.9 mPa s [9], and this is only valid when the temperature in the melt pool is constant. At any rate, for such a short time interval, which is 40 times shorter than the estimated cooling time, the latter assumption seems to be quite reasonable. However, the temperature gradient with respect to the depth results in an increase in viscosity as a function of depth, which promotes the deceleration effect due to Stoke's force. Therefore the calculated final depths are somewhat overestimated. Besides the temperature dependence of the viscosity, the convection is not taken into account. Looking at cross-sections of the laser tracks, there are no indications that convection plays an important role.

Figure 11 presents the depth at $t = 0.01$ s as a function of the injection velocity for different oxide percentages. The steepness of the graphs reveals that, provided the injection velocity is sufficient to penetrate through the surface, a relatively large depth can be reached. This explains why small changes in laser process parameters may result in a substantial change of injection depths. This is shown in Fig. 3, where an increase in the preheating temperature from 290°C to only 320°C results in a very considerable difference in the actual injection depth. For preheating temperatures higher than 440°C, the particles with the lowest speed are able to reach relatively large depths, as Fig. 3 also shows.

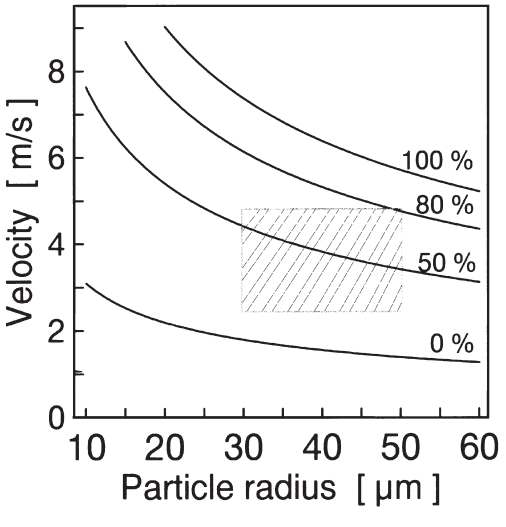

Fig. 9. Minimal particle velocity, needed to overcome the surface energy barrier, as a function of particle radius for different ratios of surface coverage by an oxide skin. The area of particle sizes and velocities in the experimental set-up is marked.

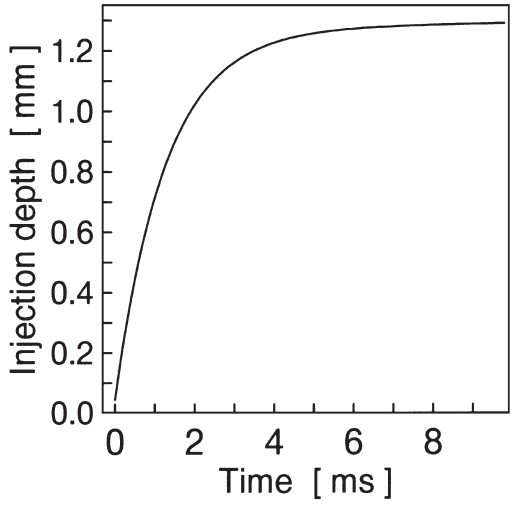

Fig. 10. Injection depth of the particle as a function of time. The injection velocity is 4 m/s, 50% of the surface is covered with an oxide skin and particle radius $R = 40$ μm.

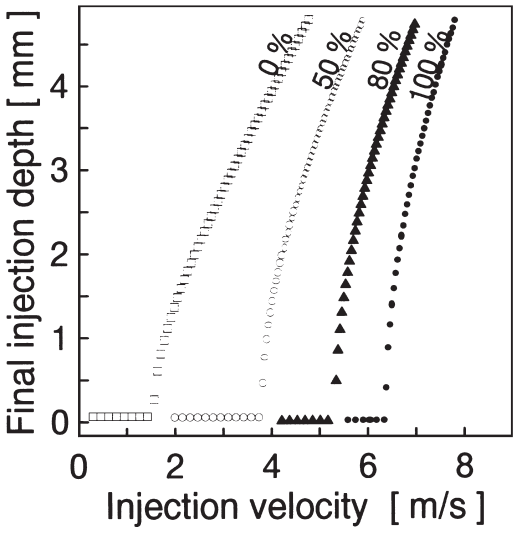

Fig. 11. Final injection depth as a function of injection velocity for different percentages of surface coverage by an oxide skin.

So, without preheating, the temperature of the melt pool is probably close to 850°C, at which the oxide skin is still present and no particles can be injected. Preheating to 290°C increases the temperature, but not high enough to remove a sufficient part of the oxide. Upon increasing the temperature further to 320°C the oxide layer is sufficiently removed to allow particle penetration. This substrate temperature increase of 30°C leads to a much higher temperature increase in the melt pool because of the better coupling factor of the laser beam at higher temperatures. In addition, the fact that we are in the temperature interval of 850–1100°C, where small temperature changes result in a substantial change in wetting behavior, explains the impact of preheating the substrate.

Indeed, the idea that the temperature of the melt pool lies in the interval 850–1100°C is supported by the fact that the particles are only injected in the center of the melt pool and not near the edges. In the center the temperature is high enough, while at the edges the temperature is too low to make any injection possible. Consequently a transition temperature from wetting to non-wetting behavior is present in the melt pool, indicating that the temperature lies in the range of 850–1100°C. The sharp transition from injection up to several hundreds of μm to no injection at all at the edges of the laser track is explained once more by the rather steep slopes in the graphs shown in Fig. 11. The increase of injection depth during laser processing (Fig. 4) is explained by the disappearance of the oxide layer as well. At the higher temperatures the decrease in kinetic energy loss during penetration of the particles through the surface causes a deeper penetration of the particles. The depth oscillations, with a frequency of 5–10 Hz as observed in Fig. 4, can be explained by the oscillatory kinetic behavior of the melt pool surface or by the oscillatory changes in the powder stream.

Other apparent solutions to create better injection conditions, i.e., besides preheating the substrate, are an increment of the laser power to increase the melt pool temperature, or to enhance the particle velocity. An increase of the laser power is not advisable because it will lead to further damage of the SiC_p and the formation of undesired Al_4C_3 [6, 17, 18]. In addition, an increase in the particle velocity may result in further damage or blowing away of the melt pool by the bombardment of particles and the strong carrier gas flow. Consequently, preheating is an efficient and elegant method to be able to inject SiC into Al.

5. CONCLUSIONS

The small parameter window for laser processing of an SiC_p/Al MMC layer on an Al substrate is caused by the large difference between the laser light absorptivities of SiC and Al as well as the presence of an oxide skin on the Al melt. The final injection depth of SiC particles in the Al melt is controlled mainly by the fraction of surface covered with oxide, i.e., by the temperature of the melt pool. A thick oxide skin on the Al melt at lower temperatures leads to a loss of kinetic energy of the particles in the wetting process, and therefore they are not able to propagate into the melt.

Preheating the substrate to above 300°C is an effective method for the successful injection of SiC particles into the Al melt, by achieving the necessary high temperatures of the melt pool at which the oxide skin is fully or partially dissolved and avoiding the use of high laser power that leads to overheating of the SiC particles.

Because of the transverse gradient of the temperature in the melt pool, SiC particles are only injected in the center area of the melt pool. The two side areas are almost fully covered by a relatively thick oxide layer. It seems not to be possible to inject SiC particles smaller than 40 μm into Al by the LMI process.

Acknowledgements—Financial support from the foundation for Fundamental Research on Matter (FOM-Utrecht) and The Netherlands Institute for Metals Research is gratefully acknowledged. K. Post, R. Vegt and J. Harkema are thanked for their assistance in the laser experiments. ESD Delfzijl is acknowledged for providing the SiC powder.

REFERENCES

1. J. Mazumder, O. Conde, R. Villar and W. Steen (ed). *Laser Processing: Surface Treatment and Film Deposition, NATO ASI Series E*, Vol. 307. Kluwer Academic Publishers, Dordrecht, 1996.
2. Abboud, J. H. and West, D. R. F., *J. Mater Sci. Lett.*, 1991, **10**, 1149.
3. De Hosson, J. Th. M., in *Intermetallic and Ceramic Coatings*, (ed). N. B. Dahotre and T. S. Sudarshan. Marcel Dekker, New York, 1999, p. 307.

4. Baker, T. N., Xin, H., Hu, C. and Mridha, S., *Mater. Sci. Technol.*, 1994, **10**, 536.
5. De Mol van Otterloo, J. L. and De Hosson, J. Th. M., *Acta mater.*, 1997, **45**, 1225.
6. Vreeling, J. A., Ocelík, V., Pei, Y. T. and De Hosson, J. Th. M., in *Surface Treatment IV*, ed. C. A. Brebbia and J. M. Kenny, Computational Mechanics Publications, Southampton, 1999, p. 269.
7. Zhou, X. B. and De Hosson, J. Th. M., *Acta metall. mater.*, 1994, **42**, 1155.
8. Pilloz, M., Pelletier, J. M., Vannes, A. B. and Bignonnet, A., *J. de Phys. IV, Coll. C7*, 1991, **1**, C117.
9. Mondolfo, L. F., in *Aluminium Alloys: Structure and Properties*, Butterworths, London/Boston, 1976, p. 108.
10. Kaptay, G., *Mater. Sci. Forum*, 1991, **77**, 315.
11. Kloosterman, A. B., Kooi, B. J. and De Hosson, J. Th. M., *Acta mater.*, 1998, **46**, 6205.
12. Kooi, B. J., Kabel, M., Kloosterman, A. B. and De Hosson, J. Th. M., *Acta mater.*, 1999, **47**, 3105.
13. Kaptay, G., *Mater. Sci. Forum*, 1996, **215–216**, 459.
14. Kaptay, G., *Mater. Sci. Forum*, 1996, **215–216**, 475.
15. Hofmann, S., in *Auger and X-ray Photoelectron Spectroscopy*, ed. D. Briggs and M. P. Seah, *Practical Surface Analysis*, Vol. 1. John Wiley & Sons, New York, 1990, p. 143.
16. Kelly, R. and Lam, N. Q., *Radiat. Eff.*, 1973, **19**, 39.
17. Hu, C., Xin, H. and Baker, T. N., *J. Mater. Sci.*, 1995, **30**, 5985.
18. Pantelis, D., Tissandier, A., Manolatos, P. and Ponthiaux, P., *Mater. Sci. Technol.*, 1995, **11**, 299.
19. Vreeling, J. A., Ocelík, V., Hamstra, G. A., Pei, Y. T. and De Hosson, J. Th. M., *Scripta mater.*, 2000, **42**, 589.
20. Pelletier, J. M., Sahour, M. C., Pilloz, M. and Vannes, A. B., *J. Mater. Sci.*, 1993, **28**, 5184.
21. Nylund, A. and Olefjord, I., *Surf. Interface Anal.*, 1994, **21**, 283.
22. Hu, C., Xin, H. and Baker, T. N., *Mater. Sci. Technol.*, 1996, **12**, 227.
23. Hegge, H. J., Boetje, J. and De Hosson, J. Th. M., *J. Mater. Sci.*, 1990, **25**, 2335.